Topological study of multiple coexisting attractors in a nonlinear system

2009 J. Phys. A: Math. Theor. 42 385102

(http://iopscience.iop.org/1751-8121/42/38/385102)

IOP PUBLISHING JOURNAL OF PHYSICS A: MATHEMATICAL AND THEORETICAL

J. Phys. A: Math. Theor. **42** (2009) 385102 (16pp) doi:10.1088/1751-8113/42/38/385102

Topological study of multiple coexisting attractors in a nonlinear system

Anirban Ray[1], **Dibakar Ghosh**[1,2] **and A Roy Chowdhury**[1]

[1] High Energy Physics Division, Department of Physics, Jadavpur University, Calcutta-700032, India
[2] Department of Mathematics, Dinabandhu Andrews College Garia, Calcutta-700 084, India

E-mail: anirban.chaos@gmail.com, drghosh-chaos@yahoo.com and asesh-r@yahoo.com

Received 18 November 2008, in final form 5 August 2009
Published 7 September 2009
Online at stacks.iop.org/JPhysA/42/385102

Abstract
Multiple attractors in a new nonlinear dynamical system recently derived from the derivative nonlinear Schrodinger (DNLS) equation describing the Alfven turbulence in magnetized plasma are analyzed in the light of geometric characterization of orbit properties, which was originally introduced by Birman and Williams and later systematized by Gilmore, Mindlin, Letellier and others. We observe that the order in which periodic orbits appear is as predicted from their symbolic sequences by the universal sequence. The observed templates of increasing complexity are organized along a spiral (which is actually a two-dimensional homomorphic projection of the original attractor). Examples of explicit templates and their variation with respect to the parameter are exhibited.

PACS numbers: 05.45.Pq, 05.45.Ac, 05.45.−a.

1. Introduction

Recently various research workers have shown a keen interest in both local and global aspects of chaos exhibited in nonlinear systems [1, 2, 3]. The global properties are best described by the topological analysis introduced by Birman, Williams, Gilmore and others. One such example is that of the Newton–Leipnik system [4]. Here in this paper, we have found a new nonlinear system from the Galerkin approximation of the derivative nonlinear Schrodinger (DNLS) equation describing Alfvin turbulence in magnetized plasma. The chaotic properties of such a system are not studied in detail. Here, our motivation is to study these attractors from a topological point of view.

In the last decade, another method concerning the analysis of the chaotic system was developed which heavily depended on Birman–William's proposed template [5]. It depends on finding the unstable periodic orbits (UPOs) embedded in the attractor and calculating the interaction between UPOs. From this information one can project the flow into a two-dimensional flow keeping all the dynamics intact. Although at the present state it can only be

used for systems embedded in three dimensions, when it is used it can yield beautiful aspects of a chaotic attractor [5–8]. This method has already been used on the Lorenz system [8], the Rössler system [9], and the Duffing system [10]. It is also used on a chaotic data set like Belousov–Zhabotinskii [11, 12] and a modulated laser system [13–16] where a relation between attractors at different forcing frequency were obtained.

Here in this communication we have considered a reduction of the usual DNLS equation via Galerkin-type approximation, to analyze the chaotic aspects of resulting ordinary differential equations (ODEs). As it usually happens, a nonlinear set of ODEs are studied with respect to the fixed-point stability, attractor and Lyapunov spectra which actually give glimpses of the local nature of chaos [17]. In order to have a better understanding of the nature of unstable periodic orbits, and their configuration inside the attractor and super-stable state, one must have an idea about how the chaotic behavior is manifested globally. So we use topological analysis on this dynamical system.

We organized the paper as follows. First we deduce the system. Then we extracted an unstable periodic orbit from the system at different parameter values. Finally, we calculated the topological invariants like the linking number and local torsion of the corresponding unstable periodic orbits at a particular parameter value. From this information we have calculated the two-dimensional projection of the hyperbolic flow corresponding to our system.

2. Formulation

The analysis of stable and unstable structures in plasma is very important from the view point of both theory and experiment. The chief motivation being the understanding of the mechanism of transition from order to chaos or vice versa. These are equally important both in laboratory and space plasma. One of the most important and difficult problems is the occurrence of turbulence in magnetized plasma, which can be attributed to the existence of an infinite number of frequencies in a particular process. Recently people have been trying to analyze the process of turbulence in the light of the strange attractor of chaotic systems. Some important work has already been done in several situations of magnetized and unmagnatized plasma. Recently the same type of investigation has been done even in quantum plasma.

The basic nonlinear equation governing the propagation of oblique Alfven waves in a magnetized plasma can be derived following the reductive perturbative procedure of Mio *et al* [18] by starting with continuity, momentum, Maxwell equations along with polytropic equation state. The equation so obtained can be written in terms of normalized variables as

$$\left(\mathrm{i}\frac{\partial}{\partial t} - \hat{\gamma}\right) B + \mathrm{i}\alpha \frac{\partial}{\partial x}(B|B|^2) + \beta \frac{\partial^2 B}{\partial x^2} = 0, \tag{1}$$

where B stands for the normalized magnetic field, $\hat{\gamma}$ is the growth or damping factor, and β, is the sign of nonlinearity and dispersion respectively. A system of three coupled ordinary differential equations are derived by substituting the following expansion for the complex field $B(x, t)$:

$$B(x, t) = \sum_{\sigma=0}^{2} B_\sigma(t) \exp\{-\mathrm{i}(k_\sigma x - \omega_\sigma t)\}. \tag{2}$$

From the linear dispersion, we have $\omega_\sigma = -\beta k_\sigma^2$ $(\sigma = 0, 1, 2)$ and $\omega_{2,3} - \omega_0 = \Delta_{1,2}$ are the phase differences. The resonance condition $2k_0 = k_1 + k_2$ is assumed. It may be mentioned that along with equation (1) we also set the Fourier transform of $\hat{\gamma} B(x, t)$ as $\gamma(k) B_k(t)$. Substituting these in equation (1) and taking k_0, k_1, k_2 components, we arrive at three nonlinear complex ODEs written as

$$\frac{\mathrm{d}B_0}{\mathrm{d}t} = \gamma_0 B_0 + \mathrm{i}\alpha k_0\{B_0|B_0|^2 + 2B_0|B_1|^2 + 2B_0|B_2|^2 + 2B_1B_2\overline{B_0}\exp(2\mathrm{i}\Delta t)\} \tag{3a}$$

$$\frac{\mathrm{d}B_1}{\mathrm{d}t} = \gamma_1 B_1 + \mathrm{i}\alpha k_1\{2B_1|B_0|^2 + B_1|B_1|^2 + 2B_1|B_2|^2 + B_0\overline{B_2}\exp(-2\mathrm{i}\Delta t)\} \tag{3b}$$

$$\frac{\mathrm{d}B_2}{\mathrm{d}t} = \gamma_2 B_2 + \mathrm{i}\alpha k_2\{2B_2|B_0|^2 + 2B_1|B_1|^2 + B_2|B_2|^2 + 2B_0\overline{B_1}\exp(-2\mathrm{i}\Delta t)\} \tag{3c}$$

where $\Delta = \frac{\Delta_1+\Delta_2}{2}$

These are a set of nonlinear ODEs obtained from the original DNLS equation by taking recourse to the Galerkin approximation, the truncation to three terms. In the absence of turbulence, a reasonable physical model is obtained by three-wave truncation of the DNLS equation.

After neglecting the other components of equation (3) because of their low amplitudes the amplitude-phase variables

$$B_\sigma(t) = R_\sigma(t)\exp(\mathrm{i}\theta_\sigma(t)), \tag{4}$$

$\sigma = 0, 1, 2$ with R_σ and θ_σ being real, are introduced in equation (3). Also we introduce

$$\psi(t) = 2\theta_0 - \theta_1 - \theta_2 - 2\Delta t. \tag{5}$$

Hence, we get the four real equations:

$$\frac{\mathrm{d}R_0}{\mathrm{d}t} = \gamma_0 R_0 + 2\alpha k_0 R_0 R_1 R_2 \sin\psi \tag{6a}$$

$$\frac{\mathrm{d}R_1}{\mathrm{d}t} = \gamma_1 R_1 - \alpha k_1 R_0 R_2 \sin\psi \tag{6b}$$

$$\frac{\mathrm{d}R_2}{\mathrm{d}t} = \gamma_2 R_2 - \alpha k_2 R_0 R_1 \sin\psi \tag{6c}$$

$$\frac{\mathrm{d}\psi}{\mathrm{d}t} = -2\Delta + \alpha[k_1 {R_1}^2 + k_2 {R_2}^2 - R_0(k_1 + k_2)] + 4\alpha k_0 R_1 R_2 - {R_0}^2[(R_2)/(R_1) + (R_1)/(R_2)k_2]\cos\psi. \tag{6d}$$

Here the four-dimensional system has two symmetries under $(R_0, R_1, R_2, \psi) \to (-R_0, R_1, R_2, \psi)$ and $(R_0, R_1, R_2, \psi) \to (R_0, -R_1, -R_2, \psi)$. This four-dimensional system can be reduced to three equations if we assume that $\gamma_1 \approx \gamma_2$ and $k_\sigma = 0, 1, 2$ are of the same order of magnitude. Using these relations, equations (6*b*) and (6*c*) are multiplied with R_1 and R_2 respectively. Then subtracting one from the other, it is found that the time asymptotic state of $R_1 - R_2$ is zero. So we can set $R_1 = R_2$ without the loss of generality. In addition if we use $\gamma_1 \approx \gamma_2$, $k_0 \approx k_1 \approx k_2$ and utilize $\alpha = \beta = -1$ and use the following new variables:

$$T = \gamma_0 t, \qquad a_0^2 = \frac{k_0}{\gamma_0}R_0^2, \qquad a_1^2 = \frac{k_0}{\gamma_0}R_1^2, \qquad \theta = -\psi, \qquad \delta = -\frac{\Delta}{\gamma_0}, \qquad \gamma = -\frac{\gamma_1}{\gamma_0}, \tag{7}$$

we get the final form

$$\dot{a}_0 = a_0 + 2a_0a_1^2\sin\psi \tag{8a}$$

$$\dot{a}_1 = -\gamma a_1 - a_0^2 a_1 \sin\psi \tag{8b}$$

$$\dot{\psi} = -2\delta + 2\left(a_1^2 - a_0^2\right) + 2\left(2a_1^2 - a_0^2\right)\cos\psi. \tag{8c}$$

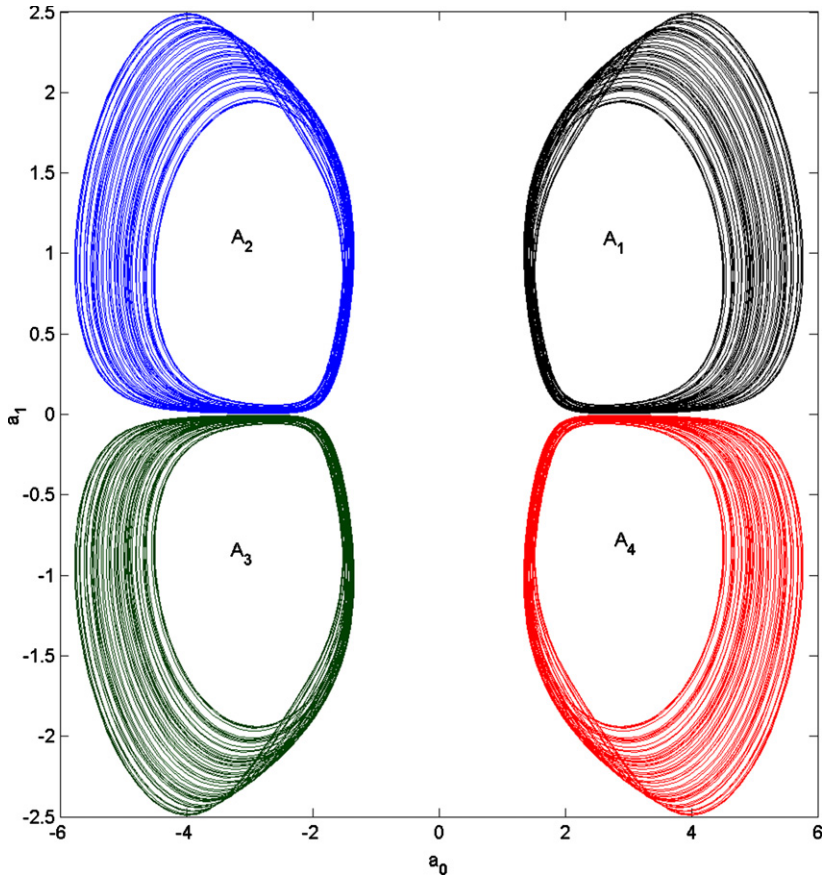

Figure 1. For parameter values $\delta = -6.02$ and $\gamma = 6.74$, attractor A_1 with the initial condition (5.556, 0.929, 3.765), attractor A_2 with the initial condition $(-5.556, 0.929, 3.765)$, attractor A_3 with the initial condition $(-5.556, -0.929, 3.765)$ and attractor A_4 with the initial condition $(5.556, -0.929, 3.765)$.

(This figure is in colour only in the electronic version)

This is the final form which we analyze from the point of view of local and global stability. Here equations (8) are invariant under a symmetry group of four operations $(a_0, a_1, \psi) \rightarrow (\pm a_0, \pm a_1, \psi)$, i.e. equation (8) has twofold reflection symmetry. As an effect of twofold reflection symmetry we get four distinct basins of attraction and four disjoined attractors as shown in figure 1 (attractors A_1, A_2, A_3, A_4) [19]. Moreover, there would be no possibility of attractor margin crisis and stretching–folding (or scrolling) will play the main role in creation of the attractors instead of tearing and squeezing mechanisms (which play the main role in Lorenz-like attractors). As these four attractors are basically the same, we will discuss the attractor A_1 and extend the results to other attractors through symmetry.

3. Bifurcation of attractor A_1

It may be mentioned that the topological approach is based on organizing the unstable periodic orbits whose linking properties severely constrain the structure of the strange attractor (figure 1 which shows the four coexisting attractors at the same parameter value).

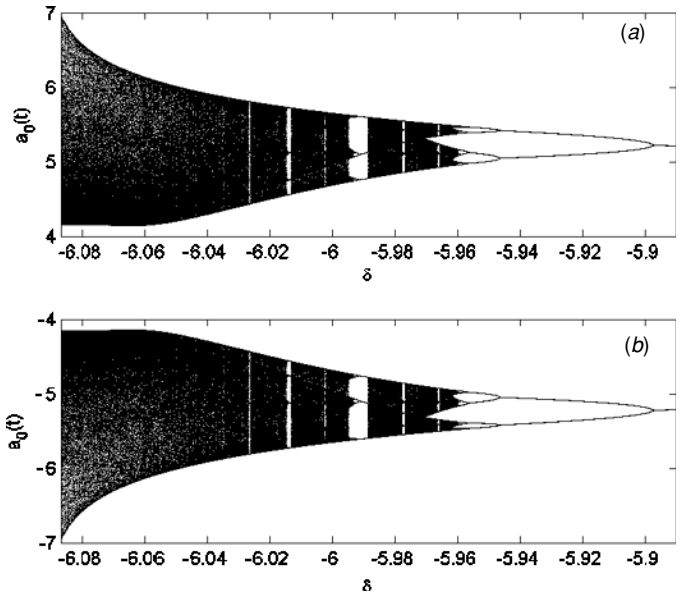

Figure 2. (*a*) The bifurcation diagram of A_1 for $\delta \in [-6.09, -5.88]$ and $\gamma = 6.74$. (*b*) The bifurcation diagram of A_2 for $\delta \in [-6.09, -5.88]$ and $\gamma = 6.74$.

A quantitative topological characterization of low-dimensional chaotic sets requires a good symbolic encoding of the trajectories which is given by first return map. We have built the FRM (first return map) at $a_1 = 1.0$ and $3 \leqslant a_0 \leqslant 6$. A mask of the attractor which may be viewed as the knot holder of the reduced plasma system is built after many visual investigations in the tri-dimensional state space. This mask is related to the stretched and folded band on which asymptotic trajectories evolve in the state space. Such an approach can be used whenever the vector field is strongly dissipative and if the Lyapunov dimension is less than 3. This method was first introduced by Birman and Williams on the Lorenz system [5]. Once the knot holder is extracted the topology is synthesized onto a template, which is described by the linking matrix M_{ij}, in which i and j run from 0 to maximum symbolic name n (for example 0 to 1 in our case).

In the last few decades several research workers have studied the characteristics of a unimodal map under the variation of the control parameter. Such a map is the actual output of the FRM. The associated symbolic dynamics of the resultant unimodal map is useful to describe the creation of periodic orbits. The method applied here are thoroughly described in [9, 20].

The initial step is an organization of the periodic orbits. Firstly one has to discard orbits which are multiples of small periodic orbits (that is, multiple encoding of the same orbit) so that one is then left with only pure or prime orbits, which can be labeled according to their order. Order is actually the integral number of periods of the simplest limit cycles or the number of distinct maxima in a_0. Our main aim is to obtain a global representation of various regimes that are encountered as the parameters (γ, δ) are varied. This can be done with the help of bifurcation diagrams which are tools commonly used in nonlinear dynamics. Such diagrams display the characteristic property of the asymptotic solution of the dynamical system as a function of the control parameter. In the case of the above system given by equation (8), derived from the plasma equation, we plot the bifurcation diagram of two coexisting attractors (A_1 and A_2) with respect to the variation of parameter δ for fixed values of γ (figure 2). One

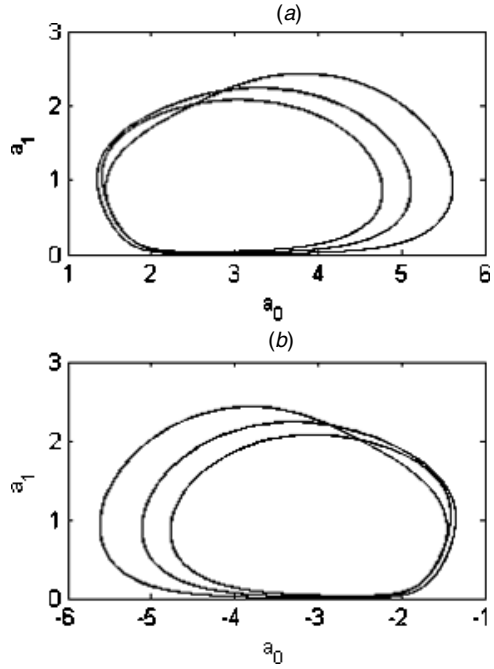

Figure 3. For $\delta = -6.004$ and $\gamma = 6.74$, (*a*) period 3 of A_1, (*b*) period 3 of A_2.

point is distinct from the bifurcation diagram that two attractors have clearly different basins of attraction. But the symmetrical nature is still evident from it. In bifurcation of A_1, values of a_0 are bounded between 4.0 and 7.0 (figure 2(*a*)). But in the case of A_2, values of a_0 are bounded between -7.0 and -4.0 (figure 2(*b*)). Here we have shown that the statement made in section 2 about the symmetry of the attractor is true. As all four of them are basically the same attractors, we have not shown the bifurcation diagram of the other two attractors. Here δ is varied in the range $\delta = -6.09$ to $\delta = -5.88$ (as shown in figure 2). It is evident from the diagram that distinguishes different periodic windows (i.e. the point from where new periodic orbits arise in the attractor) is a very difficult task. It is easy for low periodic orbits like periods 1, 2, 4, 3, 5, etc. But for higher periods these become impossible. This is where the symbolic orbit can be used. As discussed in [9, 20], each monotonic branch of the first return map (FRM) is labeled by a symbol. For the present we limit our bifurcation diagram in the range $\delta = -6.09$ to $\delta = -5.88$, where the bounded solution appears.

In attractor A_1, after $\delta = -5.8970$ period 1 orbit generates period 2 through period doubling. Then at $\delta = -5.9464$ through another period doubling we get period 4 in A_1. Then after $\delta = -5.9572$ we get period 8. These are the initial stages of period doubling cascade.

However, the structure of bifurcation is very complex. For example, the period 3 window of A_1 at $\delta = -5.9887$ and the period 5 window at $\delta = -5.9770$ are very prominent (an example of period 3 for both attractors is given in figure 3). But there are a very large number of finely interlaced windows between periodic and chaotic regimes. To analyze the bifurcation in detail we consider the symbolic dynamics. In order to introduce and take advantage of the parity of a branch in FRM, we use arithmetic symbols. The orientation-preserving branch is labeled by an even number and the orientation-reversing branch is denoted by an odd number. As an example we take the period 3 orbit in A_1; its respective interactions with the FRM are $a_{0_1} = 5.599\,494\,93$, $a_{0_2} = 4.821\,794\,51$ and $a_{0_3} = 5.221\,765\,52$. Now in our case we take the

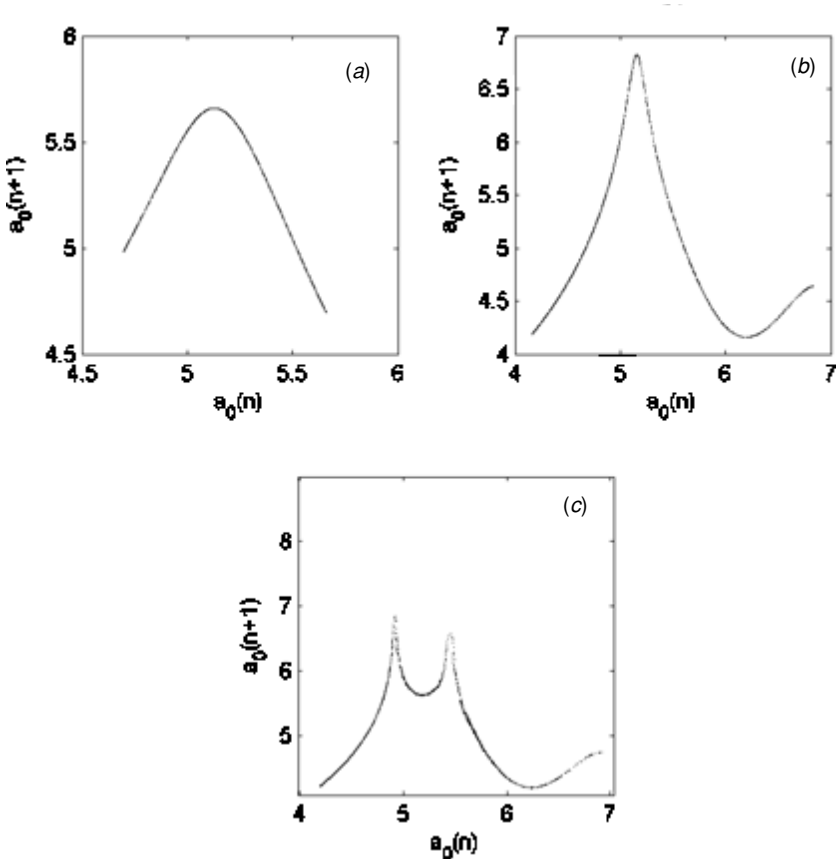

Figure 4. FRM of attractor A_1 at $\gamma = 6.74$ and (*a*) $\delta = -6.015$, (*b*) $\delta = -6.1$ and (*c*) $\delta = -6.2$.

branch on the left of $a_{0_c} = 5.1273$ as **0** and branch on the right as **1** (figure 4(*a*)). Thus, a symbol can be assigned to the orbit as $\overline{\mathbf{101}}$. Here the ordering rule employed is the same as that of [9, 20].

Now that we have defined one-dimensional symbolic dynamics we can further go into the study of the bifurcation diagrams and later to its template characterization.

We confined our study to the region $\delta \in [-6.02, -5.88]$ when $\gamma = 6.74$. In this region of δ and γ the strange attractor evolves from a fixed point to limit cycle then to strange attractor. The variation of the corresponding FRM of attractor A_1 is shown in figure 4. Here the thinness of the FRM denotes that the corresponding flow is very dissipative. So the ordering of orbit creation in the Logistic map gives essentially all the bifurcation sequences when the symbolic dynamics is binary (i.e. two symbols '0' and '1' are needed to encode the UPOs). As most periodic orbits of the dissipative system appear as predicted by a universal sequence [9, 22], we will test this in the present system. As the FRM and its variation with parameter are very similar to the Rössler system, we expect its bifurcation sequence to be very similar with that of the Rössler attractor [9]. Hence, creation of UPO in this reduced plasma system occurs according to the ordering of symbolic dynamics up to the lower order periods. They appear in the bifurcation diagram according to the ascending order within the symbolic sequence of the same length for low periodic orbits. As an example the period 7 orbits that have appeared

Table 1. Number of UPO of the lowest periods of attractor A_1 at $\delta = -6.015$ and $\gamma = 6.74$. The coordinates of the outermost point of a periodic orbit are given. The fifth column shows the torsion of the periodic orbits, sixth column shows the relative order of appearance and seventh column represented symbolic encoding of the corresponding periodic orbits.

Period	a_0	a_1	ψ	Torsion	Order	Symbol
1	5.357 840 06	0.905 667 72	3.791 630 98	1	1	1
2	5.525 817 87	0.928 838 61	3.769 224 88	1	2	10
3	4.821 840 76	0.867 784 38	3.871 840 00	2	16	101
3	4.744 380 00	0.853 055 30	3.885 792 97	1	17	100
4	5.556 121 83	0.929 127 51	3.765 589 00	3	3	1011
5	5.332 118 99	0.904 710 11	3.795 018 91	4	11	10111
5	5.281 826 02	0.904 598 77	3.801 629 07	3	12	10110
6	5.004 662 04	0.863 787 17	3.843 563 08	4	5	101110
6	5.408 620 83	0.916 463 08	3.784 445 05	5	6	101111
6	5.044 446 95	0.886 947 57	3.836 009 98	3	18	100101
7	5.568 863 87	0.930 316 21	3.764 009 00	6	9	1011111
7	5.013 860 23	0.882 452 43	3.840 859 89	5	10	1011110
7	5.506 766 80	0.918 575 23	3.772 198 92	4	24	1011010
7	4.838 449 00	0.865 651 73	3.869 306 09	5	25	1011011
7	5.152 061 94	0.896 303 42	3.819 899 08	4	27	1001011
7	5.540 403 84	0.919 946 07	3.768 064 98	3	28	1001010
8	4.912 072 18	0.869 209 71	3.857 348 92	5	4	10111010
8	5.340 314 87	0.903 004 23	3.794 070 01	6	7	10111110
8	5.418 395 04	0.917 885 78	3.783 123 97	6	14	10110111
8	5.584 825 99	0.924 039 60	3.762 542 96	5	15	10110110
8	4.860 588 07	0.870 146 99	3.865 412 95	4	21	10010110
8	5.577 506 07	0.928 263 43	3.763 130 90	5	22	10010111
9	4.889 159 20	0.872 473 18	3.860 704 90	7	8	101111110
9	4.975 214 00	0.880 880 77	3.846 782 92	6	13	101111010
9	5.505 255 22	0.916 741 91	3.772 504 09	6	19	101101110
9	5.226 480 96	0.896 018 03	3.809 648 04	7	20	101101111
9	4.805 315 02	0.863 377 57	3.874 870 06	4	23	100101100
9	5.474 557 88	0.901 191 77	3.777 251 01	5	26	100101110

in the bifurcation diagram are in the order ($\overline{1011111}$ and $\overline{1011110}$). Now if we arrange them according to the ordering rule of symbolic dynamics, then they will appear in the order ($\overline{1011111}$ and $\overline{1011110}$). Both orders are the same.

The order of appearance for the period 8 orbit is stated below. The first period 8 orbit that appears in the bifurcation diagram is $\overline{10111010}$ through period doubling; then we get $\overline{10111110}$ and $\overline{10111111}$ through saddle-node bifurcation at $\delta = 5.9674$. Later, $\overline{10111111}$ orbit gets pruned. Hence, it never appears at $\delta = -5.995$. The next candidates to occur are $\overline{10110111}$ and $\overline{10110110}$ through saddle-node bifurcation. So all the period 8 orbits of different symbolic flavors occur in the bifurcation diagram according to the ascending order of symbolic sequence. This sequence is also in symbolic order. In table 1, we have enlisted the parameter values of δ for a fixed value of $\gamma = 6.74$, after which particularly they appear. We have tested the ordering rule up to period 11 and found it to be true. This can be checked from 28 orbits up to period 9 given in tables 1 and 2.

Table 2. Occurrence of the periodic orbits of A_1 with the change of parameter $\delta \in [-6.015, -5.09]$ and $\gamma = 6.74$. Here we have used the convention P_j where P means period and j means the relative occurrence (this is a partial occurrence, i.e. after period 4_1 the period 4_2 occurs).

Period	Symbolic representation	Parameter (δ) value
2_1	10	−5.8970
4_1	1011	−5.9464
8_1	10111010	−5.9572
6_1	101110	−5.9657
6_1	101111	−5.9657
8_2	110111110	−5.9674
8_2	10111111	−5.9674
9_1	101111110	−5.9695
9_1	101111111	−5.9695
7_1	1011111	−5.9728
7_1	1011110	−5.9728
5_1	10111	−5.9770
5_1	10110	−5.9770
9_2	101111010	−5.9812
9_2	101111011	−5.9812
8_3	10110111	−5.9843
8_3	10110110	−5.9843
3_1	101	−5.9887
3_1	100	−5.9887
6_2	100101	−5.9918
9_3	101101110	−5.9942
9_3	101101111	−5.9942
8_4	10010110	−5.9961
8_4	10010111	−5.9961
9_4	100101100	−5.9973
7_2	1011010	−5.9988
7_2	1011011	−5.9988
9_5	100101110	−6.0011
7_3	1001011	−6.0032
7_3	1001010	−6.0032

The forcing rule is a powerful tool to find the occurrence of the periodic orbits in the bifurcation diagram which we have stated in table 1. The details of the rule are described in [3, 9]. It is more useful than the ordering rule. These are the relative and partial orders for the three-dimensional flow.

For each UPO, table 1 gives the coordinate of the outermost periodic points in the FRM. Three high-precession coordinates are given in this table. It may further be added that we observe the lack of the period 1 orbit of label (0). This UPO coincides with the inner fixed point. It is the first one to be created but does not lie within the attractor. The '00' symbol was absent in the symbolic sequence before the appearance of period 3 at $\delta = -5.9887$ [22]. So we can say that the attractor undergoes a change which changes its size. This is called the internal crisis. For details one could consult [23]. We did not calculate the 1D entropy

which is not relevant to these 3D flows with 2D Poincaré sections. For many orbits, 1D and 2D entropy are not the same [24].

Growing further into the parameter region $\delta \in [-6.2 - 6.02]$ (and $\gamma = 6.74$) reveals a progressive increase in the complexity of the FRM (figure 4) with the simultaneous enrichment of UPO's population. The FRMs reveal new critical points, and symbolic dynamics progressively incorporate new letters (as described by the encoding condition). Here in figure 4(c), we have shown the FRM in $\delta = -6.2$. Here two new branches occur at the FRM. This signifies that we need five-letter symbolic dynamics to encode the motion. That is, more UPOs arise inside the attractor.

It is beyond the scope of the present paper to present exhaustive results of this evaluation of the A_1 attractor. Only some typical results for the A_1 attractor are shown in table 3.

The creation of the new UPOs as the parameter 'δ' increases is a result of the growth of the attractor on the outside of the folded band. According to this the creation of periodic orbits is governed by the outermost periodic points of UPOs. Here it should be noted that to the extent to which we have searched, UPO population concerning two letter words are completed before the completion of that of three letter words (0, 1, 2). This rule is carried up to four-letter symbolic orbits that we have studied for the A_1 attractor. From these we conjecture that i-letter symbolic dynamics is completed before the completion of $(i+1)$-letter symbolic dynamics for the A_1 attractor. This is in compliance with the rules developed in [9].

4. Computation of topological invariants:

Once the UPOs are extracted from the attractor at a particular parameter value, one can go on to calculate the topological invariants [13, 15] like

(i) self-linking number and local torsion of each periodic orbit and
(ii) the linking number of the pairs of orbit.

The linking number of the two periodic orbits A and B represents how many times A winds around B. Obviously, $lk(A, B) = lk(B, A)$. If $\mathbf{X_A(t)}$ and $\mathbf{X_B(t)}$ denote the trajectories in phase space and $P_A T$ and $P_B T$ are their periods, then the linking number of A and B is the Gauss integral:

$$lk(A, B) = \frac{1}{4\pi} \int_o^{P_A T} \int_0^{P_B T} \frac{(\mathbf{X_B} - \mathbf{X_A}) \cdot (\mathbf{dX_A} \wedge \mathbf{dX_B})}{\|\mathbf{X_B} - \mathbf{X_A}\|^3}. \tag{9}$$

But it is difficult to calculate the above Gaussian integral. To our relief, this linking number can be written as

$$lk(A, B) = \frac{1}{2} \sum_i \sigma_i, \tag{10}$$

where σ_i represents the ith signed crossing between A and B. Thus, one can calculate the linking number between two orbits A and B by counting the number of signed crossings. Here σ_i is $+1$ or -1 depending on whether it is over cross or under cross. This is graphically shown in figure 5. While calculating the self-linking number for a periodic orbit A, which represents the linking of a periodic orbit with itself, we have to modify relation (10) as

$$Slk(A) = \sum_i \sigma_i. \tag{11}$$

But this self-linking number is not a topological constant in R^3 space. This is constant in $R^2 \times S$ space.

Table 3. The intersection of the UPO of the lowest periodic orbits of attractor A_1 at $\delta = -6.1$ and $\gamma = 6.74$ with the FRM and the corresponding symbolic sequence are shown.

Period	Symbol	a_0-coordinate	a_1-coordinate	ψ-coordinate
1	1	5.454 482	0.924 8986	3.783 154
2	10	5.644 196	0.919 1234	3.760 762
3	100	4.641 326	0.848 6545	3.909 968
4	1011	5.664 752	0.903 7088	3.759 351
4	1001	4.581 622	0.843 1033	3.921 254
4	1000	4.650 711	0.844 4239	3.908 612
4	2000	6.670 358	1.009 217	3.656 593
4	2001	4.547978	0.840 9672	3.927 683
5	10001	4.443 043	0.833 8637	3.948 476
5	10010	4.902 309	0.869 3106	3.864 486
5	10011	5.778 376	0.939 8175	3.744 351
5	10111	4.846 958	0.864 8170	3.873 684
5	10110	4.831 361	0.864 4527	3.876 252
5	10000	4.386 683	0.828 3781	3.960 253
5	20000	4.407 683	0.821 7251	3.956 534
5	20001	4.552 217	0.840 1238	3.926 954
6	101111	5.472 320	0.911 0307	3.781 852
6	100101	4.915 598	0.867 3168	3.862 532
6	100111	5.446 669	0.900 8806	3.785 705
6	100011	4.458 118	0.834 6265	3.945 438
6	100001	4.575 913	0.842 9812	3.922 318
6	100000	4.315 804	0.820 8312	3.975 614
6	200000	6.484 839	0.988 4309	3.673 109
6	200001	4.554 817	0.843 4123	3.926 211
6	200110	5.423 745	0.912 4944	3.787 833
6	200101	4.744 567	0.854 5670	3.891 476
7	1001111	5.780 340	0.938 0071	3.744 248
7	1000100	4.481 336	0.836 3423	3.940 770
7	1000101	5.352 275	0.909 9650	3.797 155
7	1000111	4.595 721	0.847 8810	3.918 288
7	1000011	4.860 255	0.869 1685	3.871 213
7	1000001	4.440 215	0.833 8025	3.949 044
7	1000000	4.390 615	0.829 4357	3.959 364
7	2000000	4.404 212	0.828 2123	3.956 701
7	2000001	5.239 857	0.901 7264	3.812 658
7	2000100	4.716 829	0.860 4318	3.895 791
7	2001110	5.423 796	0.896 5642	3.788 862
8	10001111	5.445 158	0.913 2339	3.785 089
8	10001100	5.753 363	0.944 0594	3.746 840
8	10000100	4.379 840	0.828 8973	3.961 607
8	10000101	4.916 883	0.866 4995	3.862 389
8	10000110	4.974 823	0.872 3711	3.852 982
8	10000011	5.964 556	0.954 8642	3.723 696
8	10000001	4.241 657	0.815 0489	3.992 134

Table 3. (Continued.)

Period	Symbol	a_0-coordinate	a_1-coordinate	ψ-coordinate
8	10000000	4.222 870	0.815 4141	3.996 271
8	20000000	5.061 439	0.883 2855	3.839 200
8	20000001	6.385 991	0.982 1149	3.682 044
8	20000010	5.579 458	0.926 0530	3.767 908
8	20001101	4.825 859	0.864 0332	3.877 196
8	20001001	4.760 636	0.858 8461	3.888 428

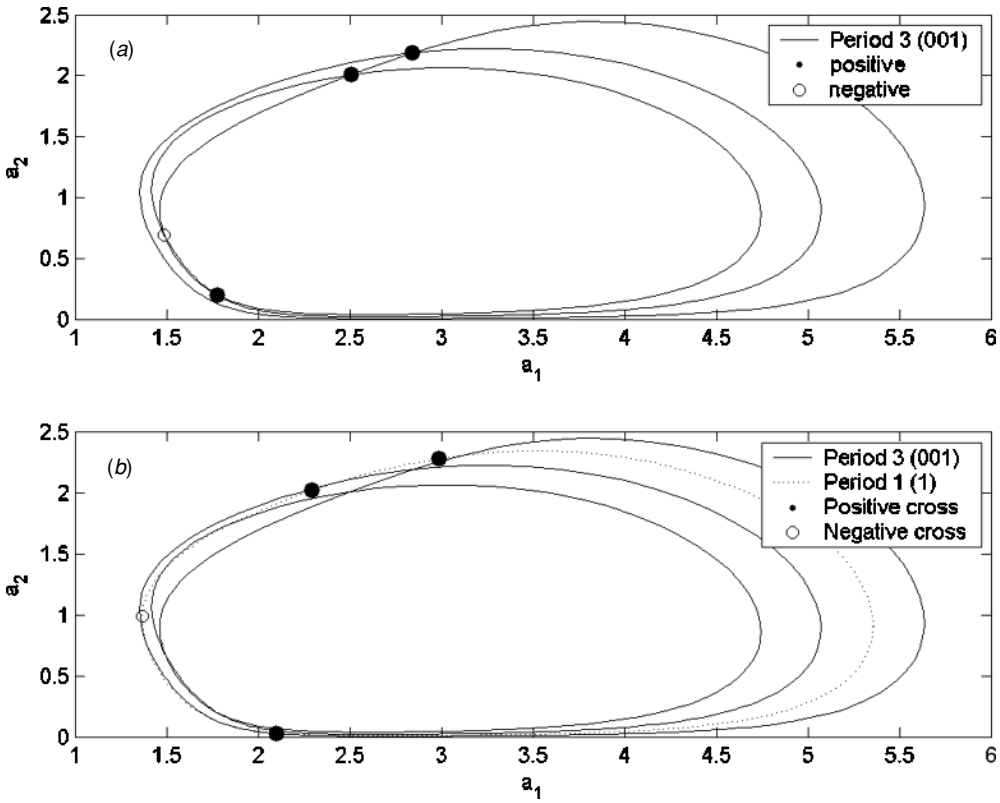

Figure 5. Example of the calculation of the self-linking number of period 3 ($\overline{100}$) and linking number between the previous orbit and period 1 ($\bar{1}$) orbit. Black dots show positive crossing and blank dots show negative crossing.

We have calculated the linking number and self-linking number of 28 orbits extracted from the dynamical system at ($\gamma = 6.54$ and $\delta = -6.015$) and they are shown in table 4. The diagonal of the table gives the self-linking number of the corresponding orbits, and off-diagonal elements give the linking number between respective orbits. An example of the calculation is shown in figure 5. In figure 5(*a*), we have three black dots and one blank dot. These dots represent the crossing points of period 3 ($\overline{100}$). The black dots are the positive crossings and the blank dots are the negative crossing. Thus, the total positive crossing number is 2. Thus, the self-linking number of the corresponding periodic orbit is 2 (from relation (11)). In figure 5(*b*), we have shown the linking between above the period 3 orbit and the period 1 orbit ($\bar{1}$). The total positive crossing number between one ($\bar{1}$) and three ($\overline{100}$) orbit

Table 4. The linking number and self-linking number of UPO of the lowest period (of A_1 at $\delta = -6.015$ and $\gamma = 6.74$) are given. UPOs are ordered in the same order as that of table 1. Here we have used the same convention P_j as described in table 2.

Period	1_1	2_1	3_1	3_1	4_1	5_1	5_1	6_1	6_1	6_2	7_1	7_1	7_2	7_2	7_3	7_3
1_1	0	1	1	1	2	2	2	2	3	3	3	3	3	3	3	3
2_1	1	1	2	2	3	4	4	4	5	5	6	6	5	5	5	5
3_1	1	2	2	3	4	5	5	6	6	6	7	7	7	7	7	7
3_1	1	2	3	2	4	5	5	5	6	6	7	7	7	7	6	6
4_1	2	3	4	4	5	8	8	8	10	10	12	12	11	11	10	10
5_1	2	4	5	5	8	8	10	10	12	12	14	14	14	14	13	13
5_1	2	4	5	5	8	10	8	10	12	12	14	14	13	13	12	12
6_1	2	4	6	5	8	10	10	9	12	12	14	14	14	14	13	13
6_1	3	5	6	6	10	12	12	12	13	15	18	18	16	16	15	15
6_2	3	5	6	6	10	12	12	12	15	13	18	18	17	17	16	16
7_1	3	6	7	7	12	14	14	14	18	18	18	21	20	20	19	19
7_1	3	6	7	7	12	14	14	14	18	18	21	18	19	19	18	18
7_2	3	5	7	7	11	14	13	14	16	17	20	19	16	18	17	17
7_2	3	5	7	7	11	14	13	14	16	17	20	19	18	16	17	17
7_3	3	5	7	6	10	13	12	13	15	16	19	18	17	17	14	16
7_3	3	5	7	6	10	13	12	13	15	16	19	18	17	17	16	14

is 2. Hence, the linking number is 1 (from equation (10)). At last, we come to the part of calculating the local torsion. Local torsion measures which way the trajectories infinitely close to a periodic orbit wind around. As one follows the UPO over one period $P_A T$, the directions of the local stable $\left(W_l^s(A)\right)$ and unstable $\left(W_l^u(A)\right)$ manifold rotate by an integer number of half turns. This number is defined to be local torsion.

In numerical simulation local torsion (Θ_l) can be computed by using linearization of the equation of motion around the periodic orbit. Given a set of ODEs

$$\frac{\mathrm{d}X}{\mathrm{d}t} = f(X, t). \tag{12}$$

The linearized equation govern the time evaluation of the infinitesimal perturbation δX of trajectory X:

$$\frac{\mathrm{d}(\delta X(t))}{\mathrm{d}t} = J(X, t)\delta X(t), \tag{13}$$

where the Jacobian matrix is given by

$$J_{ij}(X, t) = \frac{\partial f_i(X, t)}{\partial X_j}. \tag{14}$$

Given a periodic orbit $X_A(t)$ of periodic $P_A T$, and its Floquet matrix $M_A(t)$, one can always have a linear relation between $X(t + P_A T)$ and $X(t)$,

$$\delta X(t + P_A T) = M_A(t) \times \delta X(t) \tag{15}$$

can be computed by integrating equation (13) over one period of the orbit for a basis of the initial condition.

The eigenvector $\xi_s(t)(\xi_u(t))$ with the eigenvalue smaller (greater) than 1 indicates the direction of the local stable (unstable) manifold. Integrating equation (13) with the initial

condition ($\delta X(0) = \xi_u(0)$), the local torsion is then given by the formula similar to equation (9):

$$\Theta_l(A) = \frac{1}{\pi}\int_0^{P_A T} n \cdot \left(\frac{\delta X \wedge \delta \dot{X}}{\|\delta X\|^2}\right) \mathrm{d}t.$$

In our case, the local torsion of the extracted orbits is given in fifth column of table 1.

5. The template characterization

Birman and Williams have proved a remarkable theorem, which greatly facilitates the diagnosis of the dynamics of the system, which exhibits chaos and has a hyperbolic invariant set. It states that one can project all periodic orbits onto an unstable invariant manifold in the direction of stable foliation without incurring crossing. In simple terms, topological organization of periodic orbits is not changed by projection.

The attractor is the result of the stretching and folding of branches contained in the attractor. To find the topological signature we need to find the linking numbers and self-linking numbers of the UPOs among each other. The linking numbers are found by equation (10). The whole topological information about the attractor is embedded in its template. This template can be drawn from the linking number and torsion of the orbit. The template remains invariant under a small change of the parameter. But the basis set of UPOs changes.

We describe in brief the basic features of the template representation as described in [3, 7] as follows.

(i) The FRM gives the position of the attractor into N ribbon subsets and each one is labeled by the corresponding letter of the symbolic dynamics.
(ii) Each ribbon subset is carefully drawn to identify all half twist and crossings.
(iii) The template is obtained by connecting the ribbons together according to the standard insertion rules.
(iv) The $N \times N$ matrix is obtained from the knowledge of twist and crossing. Here N is the total number of distinct symbols.
(v) Each branch of an expansive template contains a period 1 orbit. The diagonal elements $T(i, i)$ of the template matrix are the local torsion of the period 1 orbit, and the off-diagonal elements $T(i, j) = T(j, i)$ $(i \neq j)$ are twice the winding number of the period 1 orbits i and j.
(vi) Finally the linking number of any two UPOs can be deduced from their symbolic dynamics.

Now in our case for the given symbolic name and its (self) linking number from tables 2 and 4, elements of the template matrix for the attractor A_1 at $\gamma = 6.74$ and $\delta = -6.015$ are given by

$$slk(01) = t_{01} + l_{01} = 1$$

$$lk(1, 01) = \frac{1}{2}t_{01} + \frac{1}{2}t_{11} + \frac{\pi(t_{11})}{2}l_{01} = 1$$

$$lk(1, 0111) = \frac{1}{2}t_{01} + \frac{3}{2}t_{11} + \frac{\pi(t_{11})}{2}l_{01} = 2$$

$$lk(01, 0111) = 2t_{01} + \frac{1}{2}t_{00} + \frac{3}{2}t_{11} + \frac{1}{2}[\pi(t_{00} + t_{11})] \times l_{01} = 3$$

$$Slk(0111) = 3t_{01} + 3t_{11} + (3 - \pi(t_{11})) \times l_{01} = 5,$$

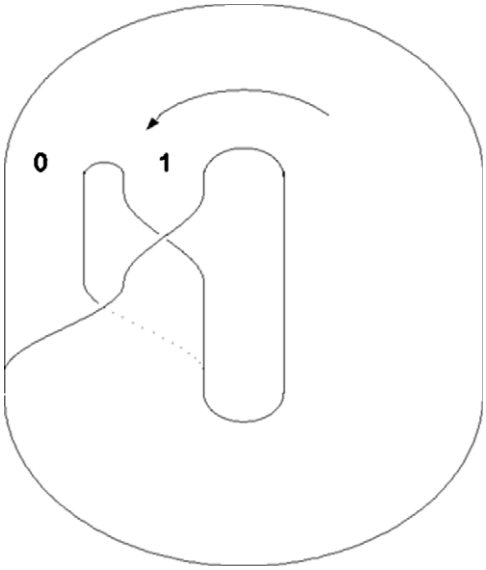

Figure 6. The two-dimensional figure of the template of A_1 represented by the template matrix and the array matrix. Two-branch template of A_1 at $\delta = -6.015$ and $\gamma = 6.74$. Here the arrow denotes the direction of the flow.

where $\pi(n) = 0$ or 1 if n is even or odd. From these equations we have the solution

$$t_{01} = 0, \quad t_{00} = 0, \quad t_{11} = 1 \quad \text{and} \quad l_{00} = 0 \quad l_{01} = 1.$$

Hence, the template can be written as

$$\begin{pmatrix} 0 & 0 \\ 0 & 1 \end{pmatrix}$$

$$(0 \quad 1).$$

Two-dimensional projection representing the above matrix is shown in figure 6. This figure shows the distinct two-branch template (one is '0' and another is '1'). As a test one can find the linking number from the template, and find that they match those in table 4.

As we progress further into the parameter region a new template arises, i.e. new branches occur. At $\delta = -6.1$ and $\gamma = 6.74$, a new branch with even parity occurs in the FRM of attractor A_1, as was described extensively in the previous section (figure 4(*b*)). Similarly a new branch with local torsion 2 occurs (i.e. it is twisted two times before coming back to FRM). Former two branches '0' and '1' keep their topology intact. Hence, the template matrix becomes a 3×3 matrix. The template matrix can be written as

$$\begin{pmatrix} 0 & 0 & 0 \\ 0 & 1 & 2 \\ 0 & 2 & 2 \end{pmatrix}$$

$$(0 \quad 2 \quad 1).$$

As we travel further into the parameter region more and more branches with even and odd parity occur in the FRM. Thus, new branches will be incorporated into the template of the

A_1 attractor. From the very beginning, we have said that A_1, A_2, A_3 and A_4 are not different. They are just the image of one another. From this we can conjecture that a template containing all other attractors would be either the same template, that explains the flow of A_1, or the mirror image of the template defined above.

6. Conclusion and discussion

In our above analysis we have studied in detail the mechanisms which are responsible for the formation of the chaotic attractor for a new chaotic dynamical system. The important aspect of the system, which is worth pointing out, is that there are four disjoined coexisting attractors arising out of the two two-fold symmetry of the governing equation. As proposed in [19], these four attractors have distinct basins of attraction and disjoined attractors which is proved with the help of figures 1 and 2. As these attractors are basically the same, we calculated the template structure of the attractor A_1 at different parameter values. All the UPOs and symbolic dynamics corresponding to each different case can be explicitly constructed. We have also seen that the periodic orbit appear as predicted by universal sequence. This study might help us to understand the behavior of these coexisting attractors.

Acknowledgments

The authors are very thankful to the suggestion of referees, who have made it possible to arrange the paper in the present form. Moreover, the authors want to thank Professor C Letellier for setting the guidelines for preparing the paper.

References

[1] Guckenhimer J and Holmes P 1983 *Nonlinear Oscillation, Dynamical System and Bifurcation of Vector Field* (Berlin: Springer)
[2] Ghrist R W, Holmes P and Sullivan M 1997 *Knots and Links in Three-Dimensional Flows* (Berlin: Springer)
[3] Gilmore R and Lefranc M 2001 *The Topology of Chaos* (New York: Wiley)
[4] Lofaro T 1997 *Int. J. Bifurcation Chaos Appl. Sci. Eng.* **7** 2723
[5] Birman J S and Williams R F 1983 *Topology* **22** 47
[6] Solari H G and Gilmore R 1988 *Phys. Rev.* A **37** 3096
[7] Mindlin G B, Hou X-J, Solari H G, Gilmore R and Natiello M A 1990 *Phys. Rev.* E **55** 5082
[8] Letellier C, Dutertre P and Gouesbet G 1994 *Phys. Rev.* E **49** 3492
[9] Letellier C, Dutertre P and Maheu B 1995 *Chaos* **5** 271
[10] Gilmore R and McCallum J W L 1995 *Phys. Rev.* E **51** 939
[11] Mindlin G B, Solari H G, Natiello M A, Gilmore R and Hou X-J 1991 *J. Nonlinear Sci.* **1** 147
[12] Mindlin G B and Gilmore R 1992 *Physica* D **58** 229
[13] Lefranc M and Glorieux P 1993 *Int. J. Bifurcation Chaos Appl. Sci. Eng.* **3** 643
[14] Boulant G, Lefranc M, Bielawski S and Derozier D 1997 *Phys. Rev.* E **55** 5082
[15] Boulant G, Lefranc M, Bielawski S and Derozier D 1998 *Int. J. Bifurcation Chaos Appl. Sci. Eng.* **8** 965
[16] Boulant G, Lefranc M, Bielawski S and Derozier D 1997 *Phys. Rev.* E **55** R3801
[17] Ray A, Ghosh D and Chowdhury A Roy 2008 *Phys. Lett.* A **372** 5329
[18] Mio N *et al* 1976 *J. Phys. Soc. Japan* **41** 1093
[19] Letellier C and Gilmore R 2001 *Phys. Rev.* E **63** 016206
[20] Hao B-L 1989 *Elementary Symbolic Dynamics and Chaos in Dissipative System* (Singapore: World Scientific)
[21] Sarkovskii A N 1964 *Ukr. Mat. Z.* **16** 61
[22] Lefranc M *et al* 1994 *Phys. Rev. Lett.* **73** 1364
[23] Grebogi C and Ott E 1983 *Physica* D **7** 181
[24] Mindlin G B, López-Ruiz R, Solari H G and Gilmore R 1993 *Phys. Rev.* E **48** 4297